Dynamic analysis of 10 MW offshore wind turbines with different support structures subjected to earthquake loadings

Yangtian Yan[1], Yang Yang[2], Musa Bashir[3], Chun Li[1, *], Jin Wang[3]

1. School of Energy and Power Engineering, the University of Shanghai for Science and Technology, Shanghai, 200093, P.R. China

2. Faculty of Maritime and Transportation, Ningbo University, Ningbo, 315211, P.R. China

3. Liverpool Logistics, Offshore and Marine (LOOM) Research Institute, School of Engineering, Liverpool John Moores University, Liverpool, Byrom Street, L3 3AF, UK

Abstract: This paper investigates the structural dynamics of 10 MW offshore wind turbines (OWTs) supported by different substructures (Monopile, Tripod and Jacket) under wind, wave, current and earthquake loadings. The support structures are modeled using ANSYS, a finite element models (FEM) software package, by considering the nonlinear soil structure interaction (SSI) effects and earthquake loadings. A spring-displacement method has been employed to model the earthquake excitations on the support structures. FAST and AQWA tools have been used to analyze wind and wave loads which are fed into ANSYS via a dynamic link library (DLL) as external loads for combination with the earthquake loads to predict the support structures' responses. Earthquakes of different magnitudes have been simulated in the study. Under the earthquake with a magnitude of 7 measured on a Richter scale, the tower top displacements of the tripod, jacket and monopile are 1.42 m, 1.75 m and 1.80 m,

respectively. The relative position of the displacement trajectory of the tripod OWT is nearest to the centroid of the yaw bearing. The maximum stresses of the jacket and tripod are respectively 5.7 times and 2.3 times that of the monopile. The average stress of the jacket and tripod are respectively 0.74 times and 0.56 times that of the monopile. This phenomenon shows that the tripod and jacket have a good stability, but with a high risk of local failure under earthquakes. The responses of the piles are mainly dominated by the seismic loads, rather than the wind and current loads. It was observed that the piles of the jacket and tripod OWT, which have small diameters and thin wall thickness, are more sensitive to earthquakes. Thus, the jacket and tripod OWTs may rely on the large stiffness offered by substructures to improve their stability. These phenomena can provide powerful insight into the seismic design of different substructures.

Key words： Offshore wind turbines; Dynamic response; Support structure; Earthquake;

1. Introduction

Global transition in energy consumption from fossil fuels to renewable and sustainable energy as an efficient means to achieving the net zero emission goal by 2050 is currently underway. The number of wind energy platforms to be installed globally is expected to contribute around 180 GW of electricity annually for wind power to become the backbone of energy systems over the world [1]. In 2019, 93 GW of newly installed wind capabilities, including 6.1 GW offshore wind, were added. Offshore wind resources, with advantages of low turbulence and slight noise, are abundantly distributed over the world. For these reasons, offshore wind turbines (OWTs)

45 are expected to significantly contribute to achieving the net zero emission goal.

46 The structural support system of an OWT consists of the tower and substructure
47 that is embedded into the seabed to provide sufficient stability. The dynamic behavior
48 of the support structure is affected by the substructure type and its soil structure
49 interaction effects [2-3]. The choice of the support structure type for an OWT depends
50 on water depth and seabed soil characteristics. For example, monopile is the most
51 commonly-used support structure in shallow water areas, while tripod and jacket types
52 are more suitable for intermediate water depth (40 ~ 60 m) applications [45-6].

53 The responses of the support structure are not only attributed to turbulent wind,
54 current, wave, and other stochastic environmental loadings (*e.g*. earthquake excitation)
55 but also influenced by the type of the support structure [7]. Numerous offshore wind
56 farms in the world are located in close proximity to earthquake-prone zones [8]. The
57 tremendous energy released by an earthquake is transmitted to the support structure and
58 several studies have been carried out on monopile OWTs, but much less on tripod or
59 jacket types. Design guidelines and recommended practices have been developed for
60 wind turbines impacted by earthquakes by the Det Norske Veritas (DNV) and Denmark
61 Risø National Laboratory, Germanischer Lloyd (GL), and the American Wind Energy
62 Association (AWEA)/ American Society of Civil Engineers (ASCE). The requirements
63 for structural modeling, load prediction approach and environmental condition
64 definition are described in these standards [9-11].

65 OWTs supported by different support structures are expected to have distinct
66 natural frequencies due to variation in geometrical configuration and structural design

of monopile, tripod and jacket. The 1st and 2nd natural frequencies of OWT are typically avoided from the selection of environmental load frequency during design [12]. Many scholars have studied the natural frequency of support structures of OWT [13-16]. Although the substructure and wind turbine are respectively designed by different manufacturers, the mode of study of their dynamic characteristics should be carried out together for proper assembling as a unit [17]. Therefore, it is important to evaluate the natural frequencies and vibration modes of OWT when investigating their dynamic responses with different support structures. Thus far, only few studies on the above problem for 10 MW OWTs with tripod and jacket have been reported.

The support structure of an OWT can be modeled in FAST using beam elements to calculate the dynamic responses with a low computational resource cost. FAST is multi-physics calculation code developed for wind turbines subjected to multiple environmental loadings. Asareh and Prowell developed a seismic analysis module within FAST to examine wind and earthquake loads [18-19]. Yang *et al.* [20] developed and validated a seismic tool, NAF (Numerical Analysis Framework) based on FAST for seismic analysis of OWTs. Jalbi *et al.* [21] studied the vibration modes of jackets supporting a 5 MW wind turbine modeled as a beam using a finite element method. Their study investigates the significance of vibration modes of for wind turbines and develops a formulation for obtaining structural optimization. Ali *et al.* [22] also used a finite element beam model to investigate the seismic response of a 5 MW wind turbine monopile. The study investigates the effects of different rotor-nacelle-assembly models on seismic failure and fragility. The support structure of the OWT is composed of

hollow steel tubes. The circumferential responses and damage of the steel tubes cannot be analyzed by a beam model. It is noted that the above studies employed a beam element method, which is only suitable for prediction of overall responses of the support structure but not an appropriate option for the investigation and optimization of local responses of OWTs.

Bazeos *et al.* [23] used a refined finite element shell elements modelling method to study the seismic behavior of a 450 kW wind turbine. Their findings show that the OWT's local buckling failure phenomenon shows the necessity to employ an elaborate model in the analysis of wind turbine structures under earthquake conditions within earthquake-prone regions [13, 24-25]. Yang *et al.* [26] studied the local design optimization of a 5 MW wind turbine supported by tripod using a finite element shell model. Their investigation reveals that it is possible to achieve a reliable OWT design that offers better dynamic performance and less weight using the model. Lana *et al.* [27] examined the dynamic response and buckling behaviour of the NREL 5 MW wind turbine made of a concrete tower using solid and shell models of finite elements. The solid and shell models in ANSYS have 20 nodes and 8 nodes, respectively [28]. The reason for using shell elements was to reduce computational time and improve simulation efficiency. The beam method was not used because it has limitations in investigating the local structural dynamics for a relatively more detailed study. The solid method requires the most computational resources, while its precision is almost equivalent to the shell model. Therefore, the shell element model is adjudged to be suitable for seismic dynamic analysis of wind turbines.

Most of the early studies on wind turbines seismic analysis methods use a response spectrum approach to estimate seismic loads. The origin of the spectrum application in the seismic analysis of OWTs can be traced to seismic codes for buildings. The load demand of a wind turbine is predicted based on a seismic response spectrum and its modal characteristics [13-2930]. Ma *et al.* [31] conducted a comparative study of the seismic responses of a 5MW wind turbine support structure predicted using a time domain analysis method and a spectral analysis method. The comparison indicated that the results obtained by the response spectrum analysis were more conservative and significantly extensive than those predicted by the time domain simulation. The wind turbine foundation employed in the study was designed in accordance with the building codes, which explains the overly conservative assessment of OWTs' seismic load. Witcher [32] found that the conventional seismic assessment method for buildings was incapable of dealing with aeroelastic and servo-control problems induced by wind turbines. The time-domain method offers the best path to solving the aeroelastic effects of wind turbines, which needs to be considered in structural investigation of OWTs.

Wind, wave and current loadings are the virtual environmentally induced excitations needed for OWTs structural design, and should be considered along with earthquake loading in the seismic analysis of OWTs [33-34]. It should be noted that high computational resources are required when calculating wind, wave and current loadings using CFD. Current design procedures for the OWTs design are more reliant on a quasi-static load prediction method [35-3637]. Sun *et al.* [38] analyzed the structural response and vibration control of the NREL's 5 MW monopile wind turbine

under combined wind, wave, and seismic loads. TurbSim program, a component of FAST, was used to generate a three-dimensional (3D) wind profile for the entire rotor domain. Aerodynamic loads acting on wind turbine blades in operation are predicted based on the Blade Element Momentum (BEM) theory. Wave-induced loading on the cylindrical structure of OWT is predicted using Morison's equation. A 3D FEM for scour analysis of an OWT's pile structure under wind, wave and current loads during normal operation was developed by Ma *et al.* [39]. Wind loads on the rotor were considered by applying them as fixed force on the tower top while the wave-induced loads on slender structural members, such as a pile, were predicted using Morison's equation. Wind-wave-earthquake uncoupled multi-physical field model was adopted for these problems. The aerodynamic load is calculated using the generalized dynamic inflow theory and BEM, and the wave load is based on the Morrison equation.

As can be concluded from the above literature review, previous studies on seismic analysis of OWTs mostly focused on the OWT with a capacity upto 5 MW. In addition, most of those studies employed the relatively coarse multibody methods to examine the structural dynamics. The relatively coarse beam method was normally used to examine structural dynamics, which is incapable of investigating the local stress concentration problem induced by an earthquake excitation. The capacity of the offshore wind turbines examined in those studies was up to 5 MW, while seismic analysis of 10 MW offshore wind turbines still has not attracted sufficient attentions. Most of the previous studies focused on monopile-type OWTs and there has been an overwhelming lack of study on offshore wind turbines with other foundation types. Therefore, it is imperative

to perform seismic analysis of OWTs supported by a tripod or a jacket because they are the most suitable foundations to be installed in intermediate water depth for large capacity OWTs. The coupled models of OWTs used in available literature were predominantly developed in previous seismic analysis tools, which simplified or ignored one or more aspects of turbulent wind, wave, current loads, and nonlinear soil-structure interaction modeling.

Therefore, this paper presents the results of investigation on the seismic responses of wind turbines supported by monopile, tripod and jacket foundation types under the combined effects of wind, wave, current and earthquake loadings. The study developed an accurate nonlinear SSI model using ANSYS FEM software and newly developed algorithm implemented via DLL and included the material properties. Modal analysis of the OWT was conducted and the results of the tower shell system are compared against reference values in order to validate the FEM proposed in this study. Time-varying responses from wave and current loadings are calculated using diffraction analysis results from AQWA and then uncoupled wind responses in FAST. These load are subsequently applied to the structure as external forces via a DLL. Consequently, the structural vibration and stress of the 10 MW OWT with different substructures subjected to environmental and seismic loadings are investigated. The results and conclusion of this investigation contribute to the efficient design and optimization of wind turbine support structures operating in earthquake-prone locations.

2. Model with different support structure

2.1 The 10 MW wind turbine model

Following a collabration between the Technical University of Denmark (DTU) and a Danish wind power enterprise, VESTAS, in the Light Rotor project in 2012, a 10 MW reference wind turbine rotor was designed [40]. The wind turbine has a blade length of 86.47 m, with a befitting tower, hub and nacelle components designed to form a complete configuration of the 10 MW DTU reference wind turbine [41]. In this research, the same 10 MW DTU reference wind turbine is adopted for investigation as the case study. Details of the 10 MW DTU reference wind turbine structural model and specific design parameters are presented in Table 1 and Figure 1.

Table 1 Key design parameters of the DTU 10 MW Reference Wind Turbine [41]

Power	10.0 MW
Blades layout	upper drift, 3
Rated wind speed/（$m \cdot s^{-1}$）	11.4
Rated rotor speed /rpm	9.6
Rotor diameter /m	178.3
Hub height /m	119
Tower height /m	115
Hub mass /kg	105,520
Blade mass /kg	41,716
Nacelle mass /kg	446,036
Tower mass /kg	628,442

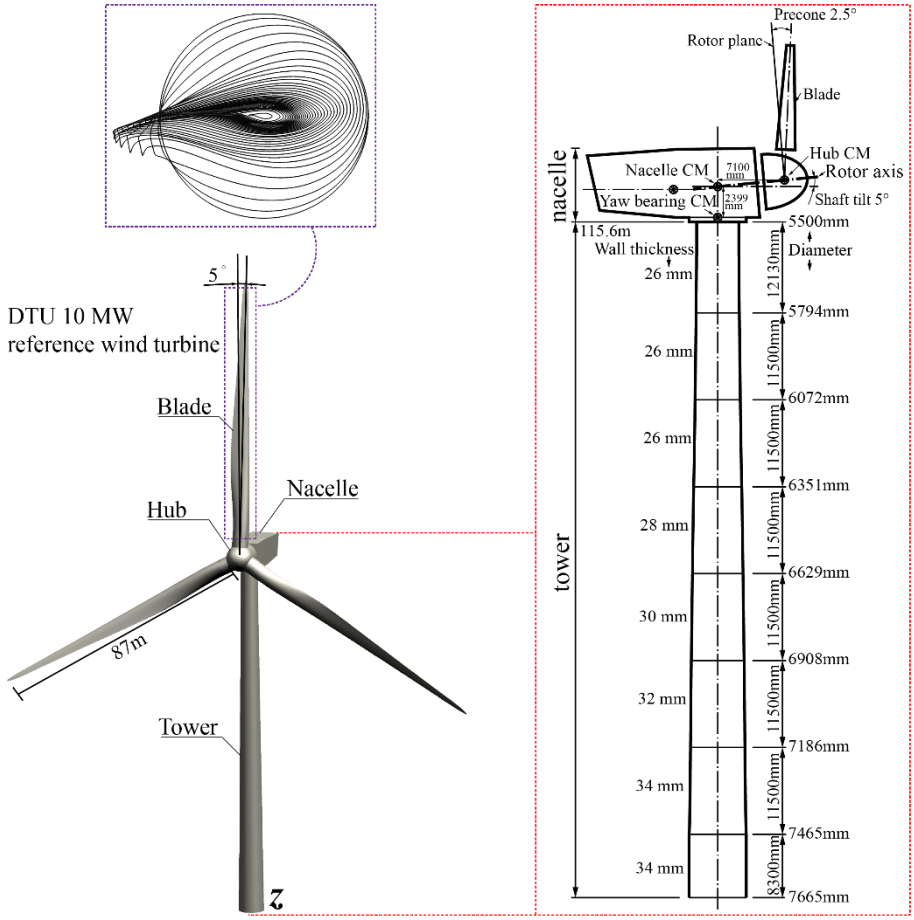

Figure 1: Structural model and support structure parameters

The wall thickness of the wind turbine's tower decreases linearly with increase in the height. Details of the dimensions show that the tower base outer diameter is 7665 mm with a wall thickness of 34 mm. The dimension of the tower top is 5500 mm diameter with a wall thickness of 26 mm. A more detailed presentation of the wind turbine support structure's parameters is shown in Figure 1, and Ref [41]. The support structure is made of grade A709 high strength structural steel material with Young's modulus and Poisson ratio of 210 GPa and 0.3, respectively. The density of the steel is chosen as 8500 kg/m^3 in order to account for the wind turbine's appurtenances such as coatings, flanges, bolts, and welding point masses that are often ignored in modeling [11].

198 A modal analysis of the wind turbine structure is performed in order to validate
199 the FEM model developed in this study. There are several methods of modal analysis
200 in ANSYS (Block Lanczos, Subspace, Reduced, Damped (full), QR Damped etc.) [28].
201 The Block Lanczos method is based on a frequency domain procedure used to analyze
202 the modal properties of the structures. A great number of eigen pairs are frequently
203 needed for seismic analysis and it is recognized as a most powerful tool for extraction
204 of a large number of eigen pairs in large-scale problems of structural mechanics.

205 In order to obtain accurate results when using the Block Lanczos method, the
206 number of modes is systematically selected to include at least 90% of the effective mass.
207 The effective mass of the i^{th} mode is evaluated using Eq. 1.

$$M_{ei} = \frac{\gamma_i^2}{\{\phi\}_i^T [M]_i \{\phi\}_i} \tag{1}$$

208 where, γ_i, $\{\phi\}_i$, $[M]_i$ are shape factor, mode shape and mass matrix for the i^{th}
209 mode respectively.

210 Note that $\{\phi\}_i^T [M]_i \{\phi\}_i = 1$ so that the effective mass reduces to γ_i.

211 The cumulative mass fraction for the i^{th} mode is:

$$M_{ei} = \frac{\sum_{j=1}^{i} M_{ej}}{\sum_{j=1}^{N} M_{ej}} \tag{2}$$

212 where, N is the number of modes.

213 The predicted natural frequencies and eigen modes of the tower are compared
214 against reference results for benchmarking, as presented in Table 2.

215

216 Table 2: The eigen frequencies of the OWT tower

	Reference [41] (Hz)	Present (Hz)
1st side-side	0.25	0.25
1st fore-aft	0.25	0.25
2nd side-side	1.97	1.91
2nd fore-aft	2.25	2.20

It can be seen in Table 2 that the eigen frequencies of first fore-aft and side-side modes of the referenced results are identical to those predicted in this study. However, a slight deviation is observed between our results for the 2nd fore-aft mode frequency and the referenced results. A plausible reason for this anomaly is that the referenced results did not consider the added effects of structural connections, although the absolute error between the present study and referenced results is within the tolerable design margin of 5% [41]. Therefore, the comparison confirms that the FEM method is well established and can be relied upon to produce credible results.

2.2 Monopile

Monopile is currently the most commonly used support structure type. Some studies show that the structure is stable, and the consumables and manufacturing process cost is low [42-43]. The monopile foundation-type typically consists of a single cylindrical steel pile whose diameter (3-8 m) is often the same as the tower base. The stability of the OWTs mainly relies on the pile-soil interaction at the bottom. With the geometrical immensity of the 10MW OWT and increase in its top mass, increase in diameter and thickness of the pile have, significant cost implication on both construction and transportation to site. The maximum pile diameter of the 10 MW OWT is about 9 m [44]. The installation method of the monopile foundation for OWT is by

piling or drilling and then connecting it to the tower or platform. Monopile foundation is sensitive to vibration and vertical loads, hence it needs caution during installation.

The 10 MW monopile is modeled using the FEM method with SHELL elements. Details of the key parameters and mesh properties of the monopile support structure model are presented in Figure 2. The complete geometry is modeled using 40926 elements and 41130 nodes.

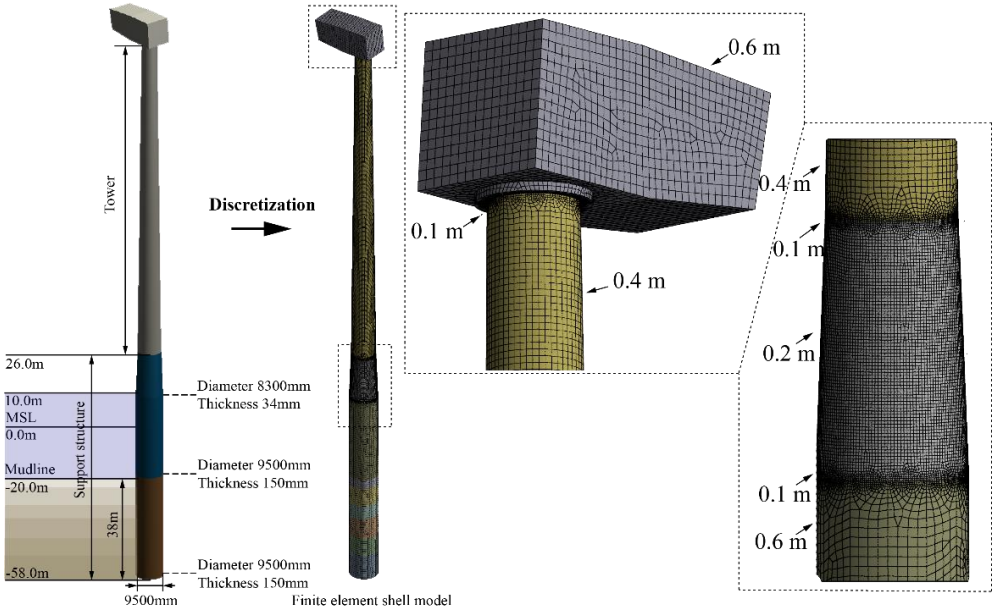

Figure 2: Discrete model and mesh properties of the 10 MW monopile [**Error! Bookmark not defined.**]

Some fundamental advantages of a monopile include easy installation procedure; a relative quick and simple manufacturing process; shorter construction period compared to other wind turbine supports; and very low requirements for seabed conditions, making it ideal for shallow water application. It is the most popular substructure alternative for shallow water locations with average water depths (<30 m) and they are not suitable for intermediate water depth (40 ~ 60 m) application due to

250 the high installation cost. The tripod and jacket types are better options for intermediate
251 water depths [4]. However, monopile has some inherent disadvantages that include
252 limited application to surface water only; large noise during installation with potential
253 negative impact on ecosystem; requirements for a large-scale tower and increase in
254 diameter and thickness of the pile once water depth increases. This further compllicates
255 installation process and the structural suitability is diminished [45].

256 *2.3 Tripod*

257 Tripods are suitable for application in transition and deep water areas whose water
258 depth is about 50 meters [4,6]. Tripod foundation consists of three steel pipe piles of
259 average diameter and arranged in an equilateral triangle. The apex of arranged piles
260 supports the upper tripod truss structure, which connects with the three steel pipe piles
261 through sleeves. Compared with the monopile, the diameter of the tripod foundations
262 is smaller, the wall thickness of the steel pile section is thin, the transportation is
263 convenient, and the material consumption is reduced [46].

264 Detailed parameters and mesh sizes of the tripod support structure are presented
265 in Figure 3. 108826 structural elements and 101416 nodes are used in modelling the
266 structure.

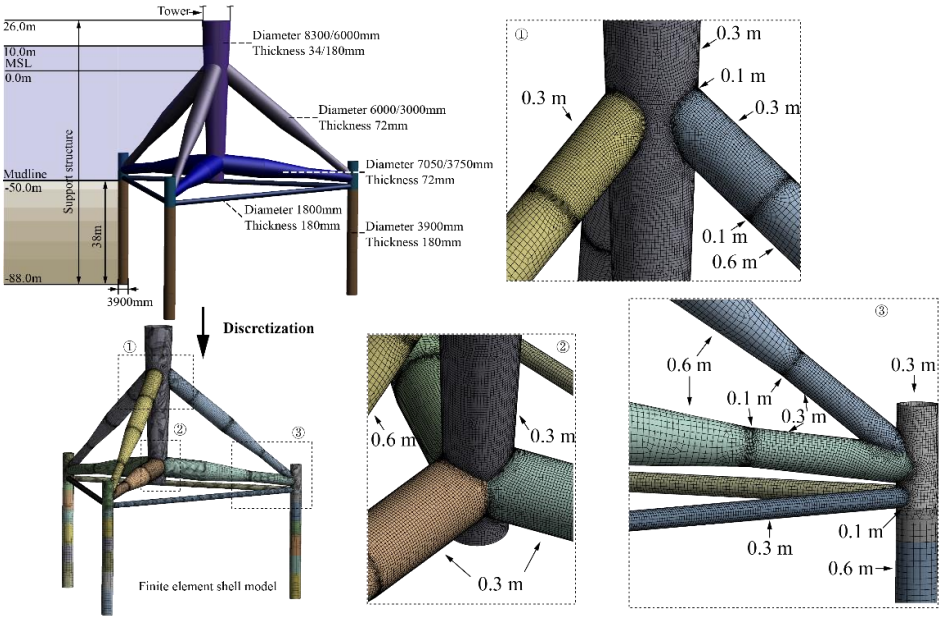

Figure 3: Discrete model and mesh properties of the 10 MW tripod [47]

Main advantages of a tripod include being light weight and of high rigidity; transportation is relatively convenient; The relative increase in cost of the structure with water depth is insignificant; Erosion protection device to prevent souring is not needed [26]. However, one disadvantage of a tripod is that each section of the hollow steel tube is connected by flange or welding making them susceptible to fatigue failure, leading to increase in installation time and complex process. The initial cost of installation of the tripod is relatively high [48].

2.4 Jacket

Although a jacket substructure is similar to a lattice structure, the jacket support needs more complex structural analysis to be performed. The foundation type is more suitable for intermediate to deep water applications. Their main advantage lies in the possibility of reaching higher depths (up to 80 m) [4]. While the monopile and tripod adopts a transition structure that connects them to the tower instead of a direct connection to the platform, a jacket is often a combined connection as a monolithic unit

283 with the tower. An innovative jacket transition structure for 10 MW wind turbines,
284 named the optimized transition piece (OTP) - Figure 4, investigated in this paper was
285 proposed in the INNWIND project [49]. The transition piece is designed as X-braces,
286 X-joints and K-joints structure. Typical height of the jacket from Mean Sea Level (MSL)
287 to the mudline is 65 m. This study adopts a jacket that has four legs and three levels of
288 X-braces. Each X-brace comprises of 12 hollow steel pipes, which are divided into two
289 types due to a difference in their diameters. The outer diameter of each steel pipe
290 gradually decreases from top to bottom.

291 The key parameters, mesh size and the K-joint parameters of the jacket support
292 structure are presented in Figure 4. The number of elements and nodes used in the
293 modelling of the jacket are 183,262 and 185,668, respectively.

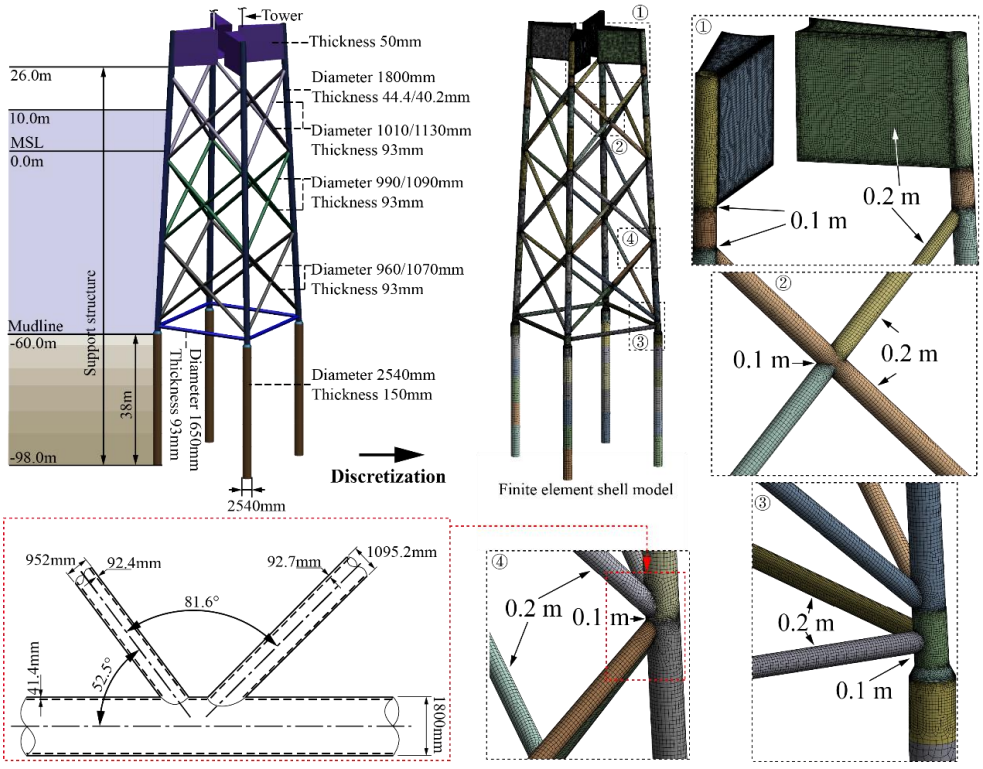

294

295 Figure 4: Discrete model and mesh properties of the 10 MW jacket [49]

296 Some advantages of a jacket platform include: high strength; high stiffness;

297 convenient transportation; suitable for large-scale wind turbines and deep water.
298 Disadvantages of a jacket include increase in material consumption with increase in
299 water depth; complex and expensive installation process; the seabed needs to be flat;
300 and corrosion protection is relatively expensive [50-52].

301 Comparing different foundations in the different water depths is based on the
302 understanding that although each foundation behaves differently, they are all designed
303 to be installed in a water depth that allows them to optimally operate. Therefore, we
304 have used each foundation type's recommended water depth as a benchmark for the
305 comparison.

306 **3. The Nonlinear boundary condition**

307 *3.1 Soil-Structure interaction model*

308 The interaction between the OWT pile and foundation soils are described by a
309 nonlinear Winkler model [40]. The pile-soil stiffness is modelled as nonlinear springs
310 in both horizontal and vertical directions based on the *p-y* and the *Q-z* curves,
311 respectively.

312 Table 3: Soil properties [40]

Depth (m)	Soil type	φ (deg)	E (MPa)	γ (kN/m3)	t_c (kPa)	t_t (kPa)	q (MPa)
-23.3	Sand	36.0	5.7	9.0	0.0	0.0	0.0
-30.0	Sand	36.0	13.7	9.0	15.1	15.1	1.1
-35.0	Sand	36.0	19.7	9.0	47.0	47.0	3.4
-42.5	Sand	36.0	24.4	10.0	71.1	71.1	5.1
-49.0	Sand	36.0	30.8	11.0	105.5	105.5	8.1

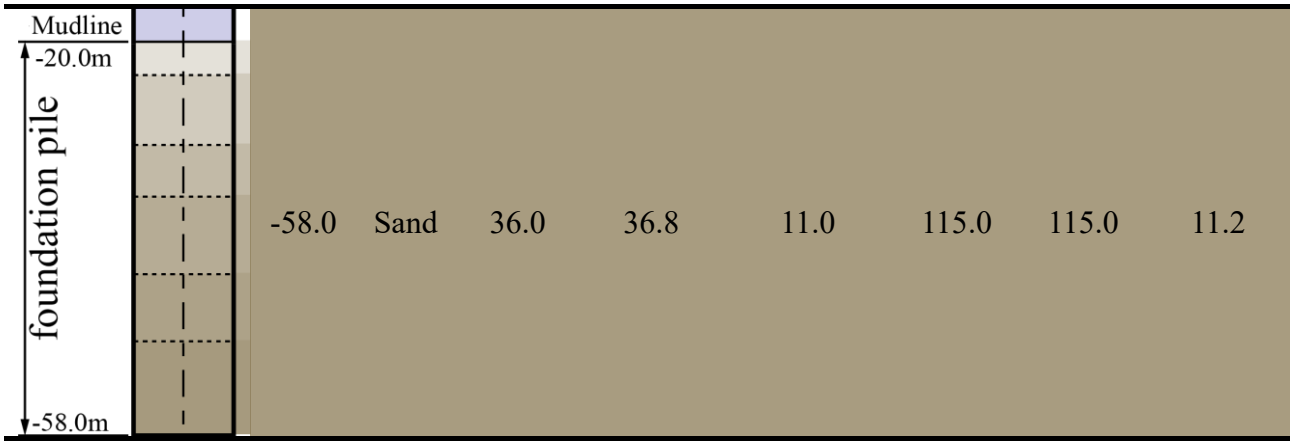

where φ is the soil's internal friction angle; E is the piles modulus of elasticity; γ is the bulk modulus or submerged unit weight. t_c is the unit skin friction compression between pile and soil. t_t is the pile-soil's unit friction tension. q is the pile's unit tip resistance (in compression).

The *p-y* curve is nonlinear and is used to describe the variation of the lateral soil resistance-deflection relationship with the embedded depth (*H*). The American Petroleum Institute (API) code for the design of a pile assumes the *p-y* relation of sand as a function of the ultimate lateral bearing capacity (p_u), that depends on soil depth, and it is presented in Eqs. (3~6).

$$p = Ap_u \tanh\left[\frac{kH}{Ap_u} y\right] \tag{3}$$

$$p_{us} = \left(C_1 H + C_2 D\right)\gamma H \quad \text{for shallow depths} \tag{4}$$

$$p_{ud} = C_3 D\gamma H \quad \text{for deep depths} \tag{5}$$

$$p_u = min\left\{p_{us}, p_{ud}\right\} \tag{6}$$

where A is a factor that accounts for cyclic or static loading conditions and its value is 0.9 for cyclic loading and for static loading, A is calculated as $\left(3-0.8\frac{H}{D}\right) \geq 0.9$; the soil reaction is denoted by p ; y is the lateral deflection (m); the ultimate bearing capacity is p_u (kN/m) at any given depth *H*; the initial modulus of subgrade reaction

is given as k (kN/m^3); H is the soil depth below mudline (m); γ is the significant unit weight of soil (kN/m^3); φ' is the internal friction angle for sand (deg); C_1, C_2 and C_3 are coefficients of a function of φ' and γ; and D is the pile diameter (m).

k and coefficients C_1, C_2 and C_3 are functions of φ'. The values of C_1, C_2 and C_3 are given as 3.2, 3.6 and 60, respectively [53]. *p-y* curves corresponding to different depths are obtained from the API standard and presented in Figure 5.

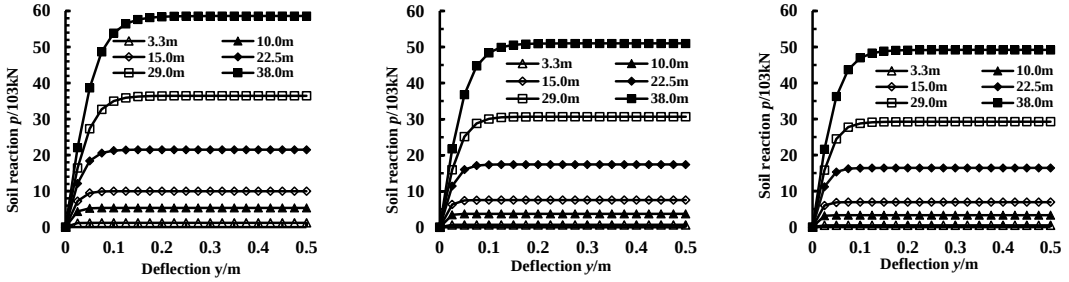

(a) Monopile (b) Tripod (c) Jacket

Figure 5: *p-y* curves of substructures at different depths

A *Q-z* curve is introduced to describe the relationship between vertical displacement and soil reaction forces. The *Q-z* curve for a monopile in clay soils and with a flat tip that offers an appreciable installation resistance at any given monopile tip depth (*z*) is calculated by using Eqs. (7-9).

$$Q = Q_s + Q_p \tag{7}$$

$$Q_s = A_w \cdot \left(\alpha_i \; Su_{DSS}\right)_{AVE} \tag{8}$$

$$Q_p = \left(N_c \cdot Su_p^{AVE} + \gamma' \cdot z\right) \cdot A_p \tag{9}$$

where Q is the total penetration resistance of the pile; Q_s is the skin resistance along the circumference of the pile; Q_p is the pile tip resistance; A_w is the total wall (pile) surface (inside and outside) area embedded into the soil area; A_p is the pile tip cross

sectional area; α_i is an adhesion factor to be applied during installation; Su_{DSS} is a simple shear strength; $\alpha_i\, Su_{DSS}$ is the skin friction of pile circumference; $(\alpha_i\, Su_{DSS})_{AVE}$ is average circumferential friction of the pile from mudline to depth z; N_c is the foundation's bearing capacity factor; Su_p^{AVE} is average of triaxial compression; γ' is the effective unit weight of soil; z is the pile tip penetration depth. The *Q*-*z* curves for the substructures being investigated in this research are obtained by using the API standard as presented in Figure 6.

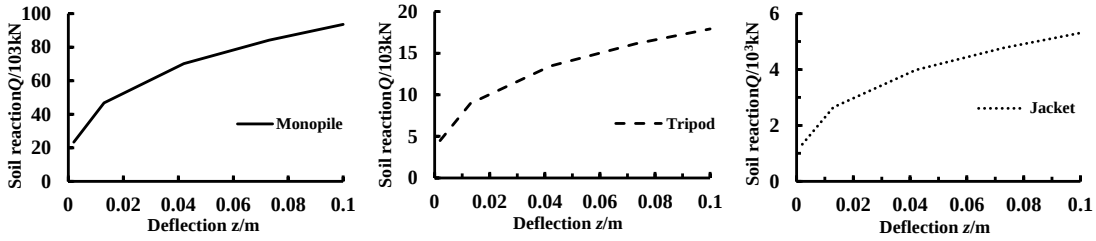

Figure 6: *Q*-*z* curves at the pile top

The interaction between the OWT structure and foundation needs to be considered as a monolithic structure in order to check its stability by accounting for the flexible OWT system. This is essential in the design and operation of the OWT because of the inherently different survivability criteria for the support structures at both seabed level and tower top. Furthermore, the soil mechanical properties are very different from the steel material used for the pile foundation. The embedded length of the pile foundation is the source of the OWT's structural stability through its design life and operation. Consequently, the seabed soil characteristics significantly influence the pile foundation dynamic behaviours.

In order to address the issues observed above, a modal analysis of the OWT structure supported by a flexible foundation is modeled using the Winkler approach to

358 establish a preliminary knowledge of SSI effects on the structure. The predicted natural
359 frequencies of the OWT's first and second modes in both fore-aft and side-side
360 directions are compared to a rigid-foundation model's, and the results are presented in
361 Table 4.

362 Table 4 Natural frequencies of the first and second modes of the OWT support structure

		No SSI (Hz)	SSI (Hz)	Error
Monopile	1st side-side	0.21	0.20	7.83%
	1st fore-aft	0.22	0.20	7.87%
	2nd side-side	1.52	1.16	23.56%
	2nd fore-aft	1.57	1.19	24.17%
Tripod	1st side-side	0.26	0.26	0.86%
	1st fore-aft	0.26	0.26	0.87%
	2nd side-side	1.77	1.27	28.41%
	2nd fore-aft	1.81	1.31	27.82%
Jacket	1st side-side	0.23	0.21	10.62%
	1st fore-aft	0.23	0.21	10.71%
	2nd side-side	1.40	1.09	22.03%
	2nd fore-aft	1.44	1.16	19.23%

363

364 It is observed from Table 4 that the SSI model has lower natural frequencies than
365 the rigid model (without SSI) does. A 7.8% relative deviation of the natural frequency
366 of the model with flexible foundation (with SSI) is produced in the 1st-mode. However,
367 a larger error of more than 23% is observed between the 2nd-mode frequencies of
368 flexible and rigid foundation models. This confirms that the SSI effects significantly
369 influence the natural modes of the OWT. Vibration and mode shapes of the OWTs with
370 both rigid and flexible foundations are presented in Figure 7. It is observed that the SSI
371 effects have a weak influence on the 1st-mode shapes while the 2nd-mode shapes display
372 a different behaviour at the tower top and nacelle.

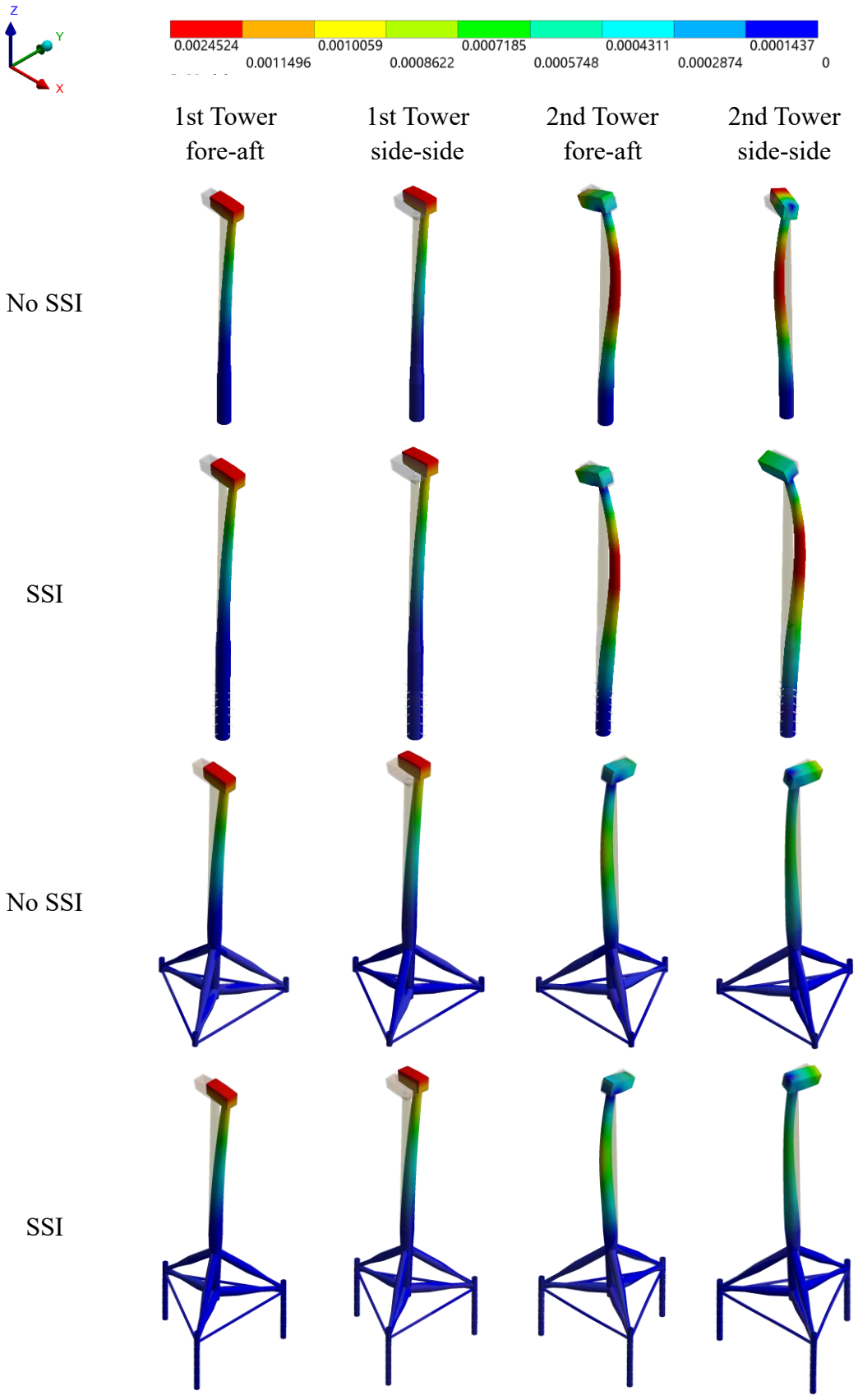
Z
Y
X
0.0024524
0.0011496
0.0010059
0.0008622
0.0007185
0.0005748
0.0004311
0.0002874
0.0001437
0
1st Tower fore-aft
1st Tower side-side
2nd Tower fore-aft
2nd Tower side-side
No SSI
SSI
No SSI
SSI

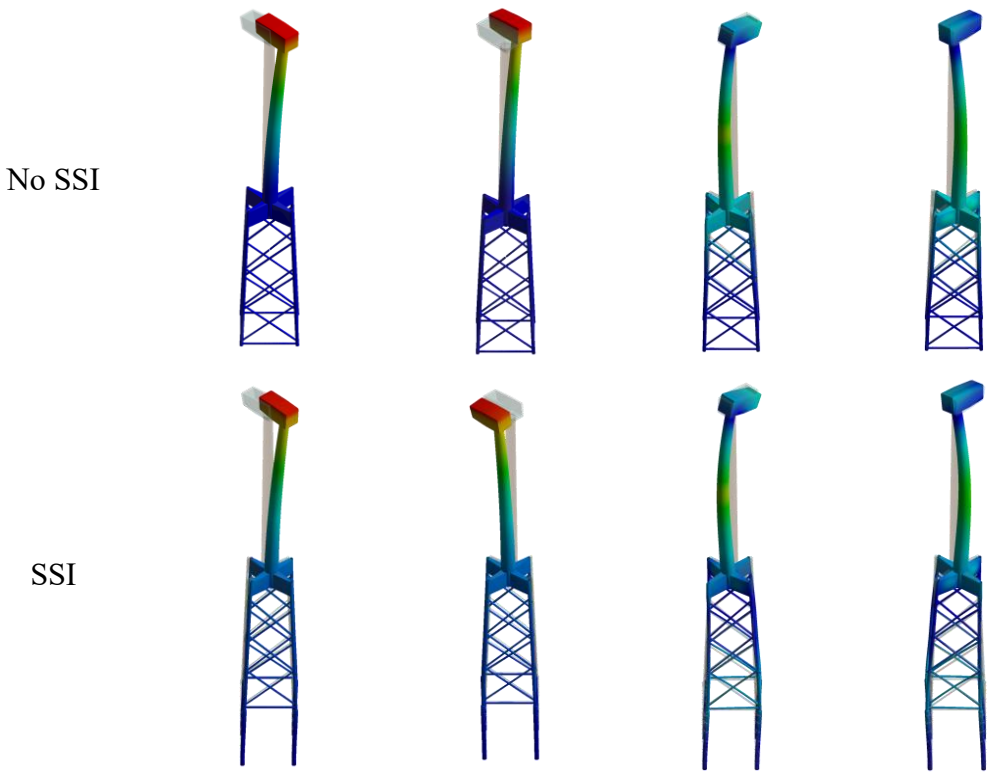

Figure 7: Mode shapes of OWTs with and without SSI for both simplified and original models

4. Environmental conditions

As shown in Figure 8, OWTs typically suffer from turbulent wind and extreme wave and current loadings during an earthquake event. The aerodynamic forces induced by wind and the wave and current generated hydrodynamic loads are respectively calculated using FAST and AQWA tools. The combined aerodynamic and hydrodynamic predicted loads are then applied as external forces to the FEM developed in ANSYS via a DLL. The turbulent wind domain of 250 m×236 m is created in the FAST model to cover the rotor sweep area. The rotor thrust acting on the OWT's hub is equally predicted using FAST while the Morison's equation in AQWA is used to calculate the wave and current loads. The seismic load acting on the pile is modelled in ANSYS using a spring-damper sytem by defining the springs' ground motion

displacement and stiffness. All relevant descriptions of the environmental loadings and associated conditions are presented in Sections 4.1-4.3.

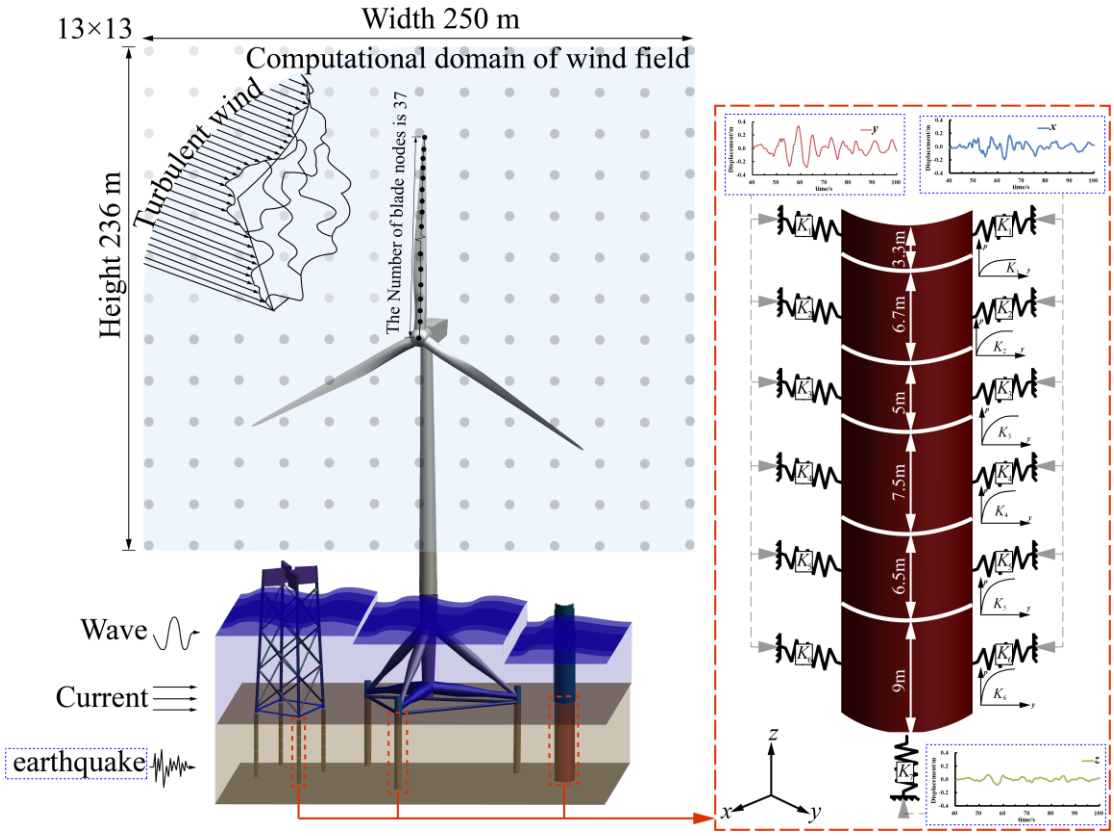

Figure 8: A model of the environmental conditions

4.1 Turbulent wind field

This investigation used the Kaimal wind spectrum model to generate the wind field's turbulent condition. The spectral density of the wind speed is calculated using Eq. (10):

$$S_K(f) = \frac{4\sigma_K^2 L_K / \bar{u}_{hub}}{(1 - 6fL_K / \bar{u}_{hub})^{5/3}} \tag{10}$$

where K represents the wind component and f is the angular frequency; L_K is a velocity component that represents the critical parameter; σ is the standard deviation of the wind speed; $\bar{u}_{hub}$ is the mean hub height wind speed. The rotor thrust predicted

using FAST for rated (11.4 m/s) and shutdown (25 m/s) conditions of the OWT are presented in Figure 9. The predicted rotor thrust is applied as a fictive force at the hub and along the rotor shaft axis.

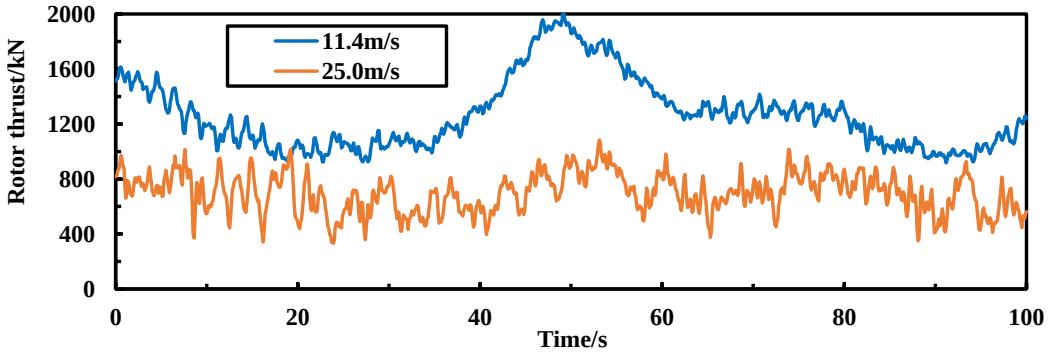

Figure 9: Rotor thrust

4.2 Wave and current

Hydrodynamic forces acting on the cylindrical pile supporting an OWT are calculated using Morison's equation given in Eq. (11):

$$F_{wave} = \frac{\pi}{4}\rho C_M D^2 \dot{u}_{wave}(t) + \frac{1}{2}\rho D C_D u_{wave}(t)\left|u_{wave}(t)\right| \tag{11}$$

where wave-induced particle velocity and acceleration are respectively denoted as $u_{wave}(t)$ and $\dot{u}_{wave}(t)$; D is the diameter of the OWT wetted structural member; C is the hydrodynamic mass coefficient and it is equal to 1.0 for circular cylinders, C_D is the drag coefficient, C_M is the inertia coefficient; F_{wave} is the total wave-induced force acting on OWT per unit length; ρ is the density of seawater.

The current-induced load was not evaluated separately from the wave load due to nonlinearity in the drag term.. However, since the direction of wave particle and current velocities is opposite for half of the wave cycle, it is essential to calculate the velocity term u^2 as the total velocity ($u_{wave}+u_{current}$) multiplied by its absolute value as shown in Eq. (12):

412 $$F=\frac{\pi}{4}\rho C_M D^2 \dot{u}_{wave}(t)+\frac{1}{2}\rho D C_D\left(u_{wave}(t)+u_{current}\right)\left|u_{wave}(t)+u_{current}\right| \quad (12)$$

413 For the wave calculation, the Peirson-Moskowitz (P-M) spectrum is chosen and

414 its semi-empirical spectrum equation is given in Eq. (13):

$$S(\omega)=\frac{0.78}{\omega^5}\exp\left[-\frac{3.11}{\omega^4 H_s^2}\right] \quad (13)$$

415 where ω is the frequency of wave; H_s is the significant wave height.

416 The significant wave height and period of the wave condition used in this study

417 are 4 m and 7.2 s, respectively. A representative wave (P-M) spectrum of the above

418 wave condition is presented in Figure. 10. Figure. 11 presents the time series of the

419 wave force predicted using AQWA.

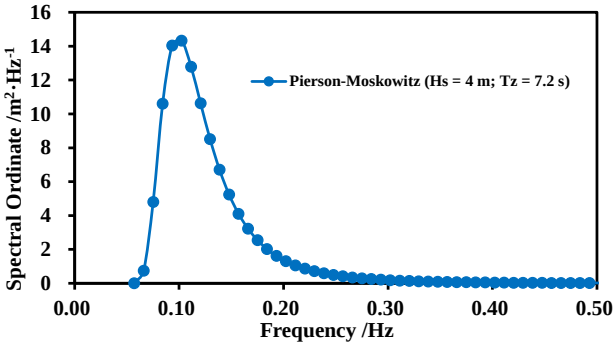

420

421 Figure 10: The wave spectrum

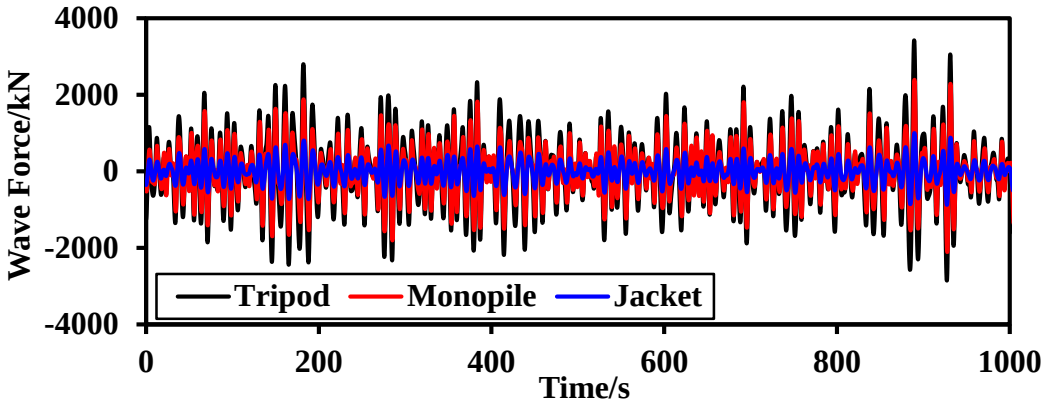

Figure 11: Wave loads

4.3 Ground motions

The ground motions with different magnitudes are selected in this study to investigate the seismic characteristics of the 10 MW OWT with different support structures. The magnitudes of the ground motion are 7.62 Ms, 6.69 Ms and 5.77 Ms. Plots of the spectral displacements and time-varying responses of the horizontal and vertical components of the earthquake are shown in Figure 12. The magnitude of the earthquake and the corresponding peak ground acceleration (PGA) are shown in Table 5.

The seismic load derived from the ground motion displacement offers the best platform to accurately describe the process of seismic energy transfer from soil to pile. For this reason, the ground displacements, which have similar responses to the PGA have been selected. The Chi-Chi earthquake with a Richter scale magnitude of 7.62 Ms and PGA of 6.08 m/s^2, Northridge-01 earthquake with a Richter scale magnitude of 6.69 Ms and PGA 6.86 m/s^2, and the Coalinga-05 earthquake with a Richter scale magnitude of 5.77 Ms and PGA of 7.06 m/s^2, were examined. A plot of the selected earthquake records showing the spectrums of their displacement along *x*, *y* and *z* axes are shown in Figure. 12.

From the record, it was established that the peak ground displacement (PGD) of 7.62 Ms, 6.69 Ms and 5.77 Ms had corresponding peak periods of 15.05 s, 3.18 s and 1.94 s, respectively. It should be noted that the earthquake occurred within 40 s after initiation. Therefore, the time when the above three seismic loads reach their maximum value during calculation is 55.05 s, 43.18 s and 41.94 s, respectively

444 Table 5 Earthquake parameters

Earthquake name	Place	Year	Station	Magnitude (Ms)	PGA (g)
Chi-Chi	China	1999	TCU071	7.62	0.62
Northridge-01	America	1994	Sylmar-Converter Sta	6.69	0.70
Coalinga-05	America	1983	Oil City	5.77	0.72

445

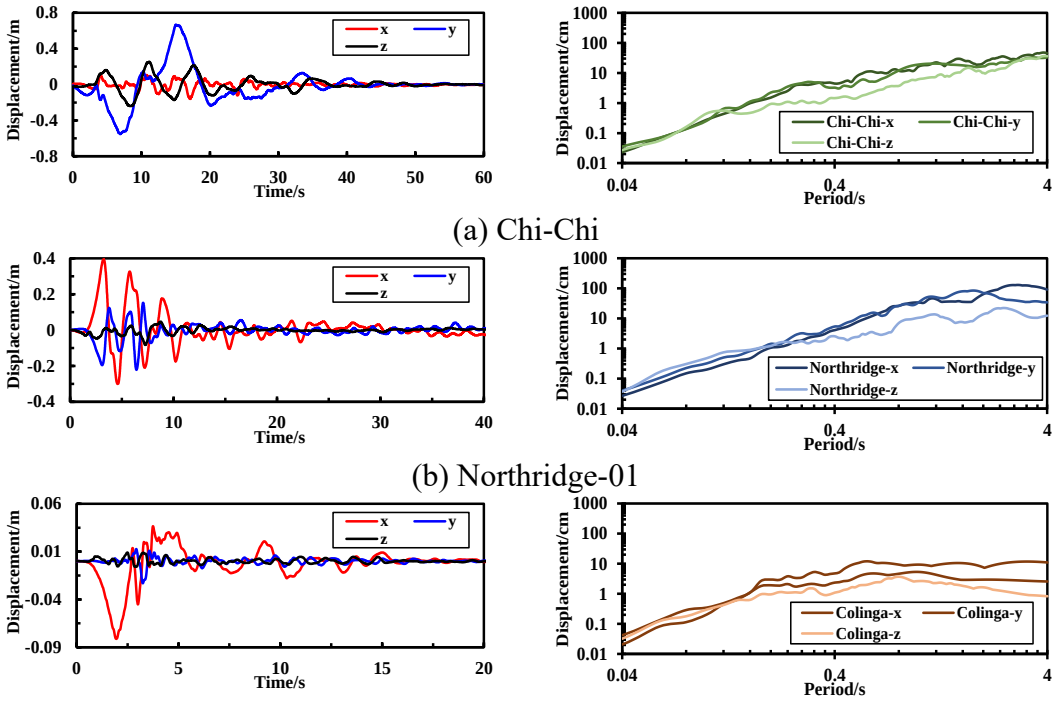

(a) Chi-Chi

(b) Northridge-01

(c) Coalinga-05

Figure 12: Displacement and spectra of ground motions along the *x*, *y*, and *z* directions

446 **5. Results and Discussions**

447 The duration of the simulation for the OWT with different support structure being
448 investigated in the study is 100 s and the corresponding load step is set at 0.01 s. Each
449 time step is further divided into two sub-steps with a time-step of 0.005 s. The wind
450 turbine turns on from 0 s and the wind loads for the rated (11.4 m/s) and cut-out (25.0
451 m/s) wind speeds are considered. In addition, only a wave and a current records are
452 considered in the simulations. This is because the earthquake is assumed to have
453 occurred at the 40th second after initiation for each load case. In total, three earthquake
454 conditions are considered and a total of 24 environmental conditions have been

simulated under different loading combinations as presented in Table 6. The computational duration of each simulation is about 36 hours on a workstation with 24 CPU cores.

Table 6 Specific environmental conditions

Case Number（Monopile）	Case Number（Tripod）	Case Number（Jacket）	Turbulent wind /m·s^{-1}	Ground motion /Ms
1	9	17	11.4	-
2	10	18	25.0	-
3	11	19	11.4	7.62
4	12	20	25.0	7.62
5	13	21	11.4	6.69
6	14	22	25.0	6.69
7	15	23	11.4	5.77
8	16	24	25.0	5.77

5.1 Dynamic analysis

5.1.1 Wind loads response

The stability of the nacelle and blades is discussed along with the vibration of the tower top. Figure 13 presents the time domain responses of tower top displacement along the *x*, *y* and *z* directions for monopile, tripod and jacket under 25.0 m/s (cut-out) and 11.4 m/s (rated) in turbulent wind condition. It corresponds to cases 1, 2, 9, 10, 17 and 18 in Table 6.

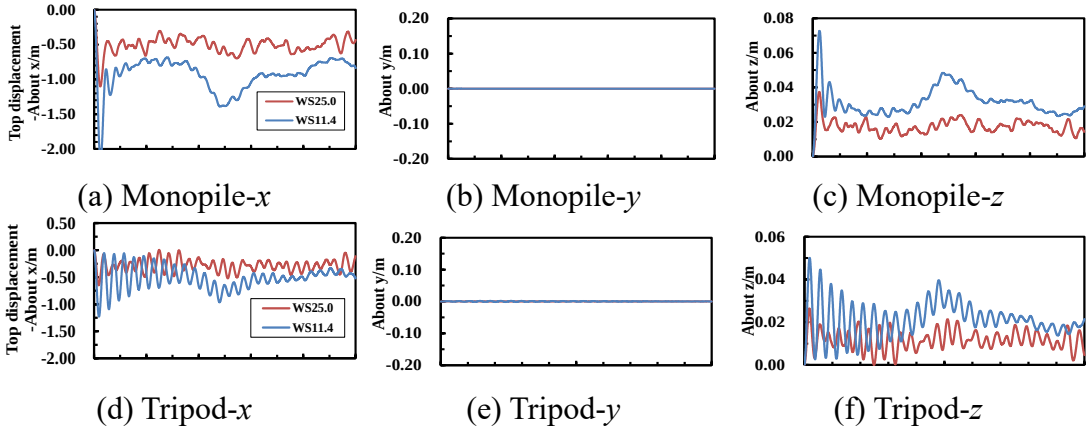

(a) Monopile-*x* (b) Monopile-*y* (c) Monopile-*z*

(d) Tripod-*x* (e) Tripod-*y* (f) Tripod-*z*

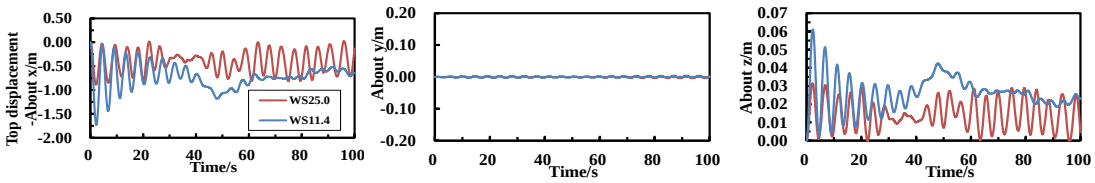

(g) Jacket-*x* (h) Jacket-*y* (i) Jacket-*z*

Figure 13: Time domain response of *x*, *y* and *z* displacement of the tower top with different support structures

As presented in Figure 13, it was observed that the tower top suffers a severe off-centre reciprocating motion along the *x* direction, which was caused by the turbulent wind condition. The displacement of each structure in the *x* direction is negative. Under the rated wind speed of 11.4 m/s, the maximum tower top displacement of the monopile is -2.15 m, which is the largest among all the supporting structure and their average is -0.93 m. The fluctuation of responses at the rated wind speed is higher because the aerodynamic load in the rated condition is correspondingly the largest. The servo system results in a smaller wind thrust on the support structure under the cut-out wind speed of 25.0 m/s. In this (cut-out) wind condition, the maximum tower top displacement of monopile structure is -1.10 m, showing a decrease of 49% when compared to the results of 11.4 m/s (rated) wind condition. When the OWT is operating at rated wind speed of 11.4 m/s, the maximum tower top displacements of tripod and jacket are -1.23 m and -1.72 m, respectively. However, when the wind speed changes to cut-out (25.0 m/s) condition, the response amplitude decreases by 47% and 48%, respectively. The maximum vertical tower top displacement shows the same trend in the *x* direction, but with a significantly smaller magnitude.

According to the above analysis, the turbulent wind load causes the tower top of the support structure to move away from the centre of motion in the wind direction. Compared with the three supporting structures, the responses of the tripod and jacket

485 structure are smaller in magnitude than that of monopile. This phenomenon shows that
486 the structure is stable. Therefore, when investigating the wind load response, the *x*
487 direction response should be the main ones to be considered. The variation of structural
488 response amplitude caused by wind loads of different support structures is similar.

489 *5.1.2 Seismic loads response*

490 The tower top displacements of the monopile OWT under the rated wind speed
491 and combined with seismic loads caused by different intensity earthquakes are
492 presented in Figure 14.

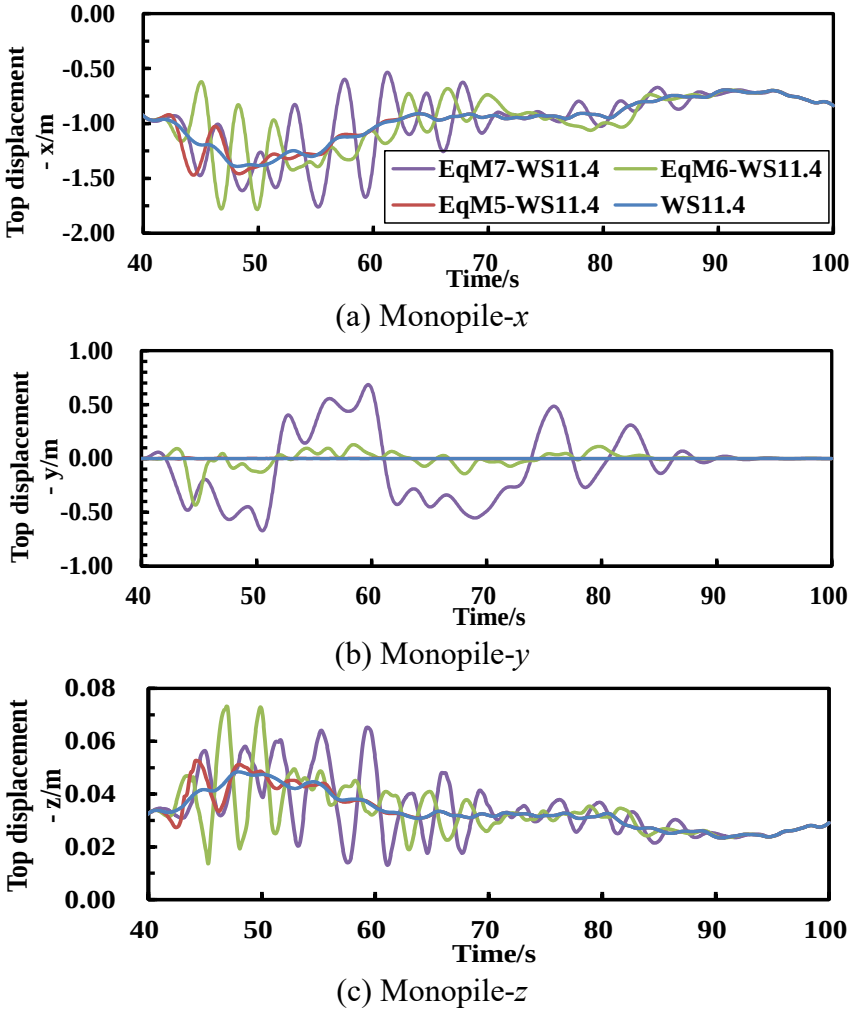

Figure 14: Time domain responses of the monopile tower top displacements along *x*, *y* and *z* axes

493 The variation in trend of the top tower displacements of monopile caused by these

494 ground motions is similar to each other. The monopile OWT with the most severe
495 displacement response is shown Figure 14.

496 The tower top displacement is discussed based on the three directions, *x*, *y* and *z*
497 considered in the simulations. The irregular displacement of the tower top in the *x*
498 direction under wind load, the displacements of the *y* and *z* directions are almost 0 m.
499 The tower top displacements in all directions fluctuate severely because of the impact
500 of the earthquake. The maximum tower displacement without an earthquake is 1.39 m,
501 while the corresponding values are 1.47 m, 17.9 m and 1.80 m under the M5, M6 and
502 M7 earthquake excitations, respectively. This means that the three earthquakes produce
503 an increase of maximum displacements by 5.82%, 28.62% and 29.22%, respectively.
504 In addition, this indicates that the maximum tower top displacement nonlinearly
505 increases with earthquake magnitude.

506 The tower top trajectory constituted by the positions of the *x* and *y* direction of the
507 monopile, tripod and jacket OWTs under earthquake is shown in Figure 15. The
508 positions of these trajectories in the *x* and *y* directions of each structure under different
509 loads and displacements relative to the centroid of yaw bearing (0 m, 0 m) load are
510 compared. The location of the centroid of the yaw bearing is shown in Figure 15. In the
511 legends of Figure 15, "EqM7+WS25" means earthquake magnitude 7 combined with
512 wind speed 25.0 m/s. "WS25" means wind speed 25.0 m/s and no earthquake.

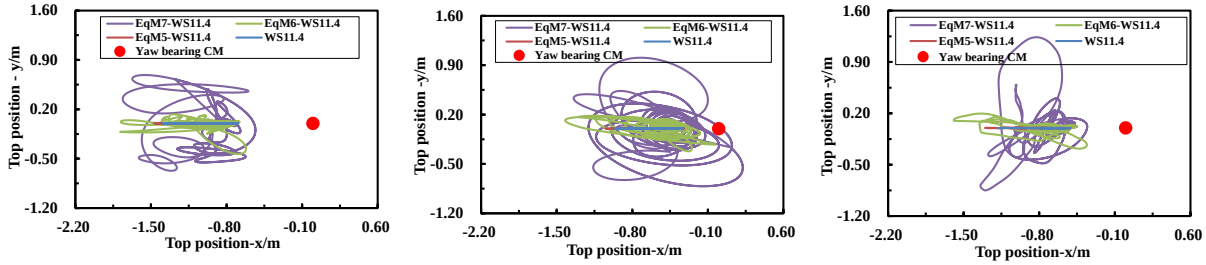

(a) Monopile-WS11.4 m/s (c) Tripod-WS11.4 m/s (e) Jacket-WS11.4 m/s

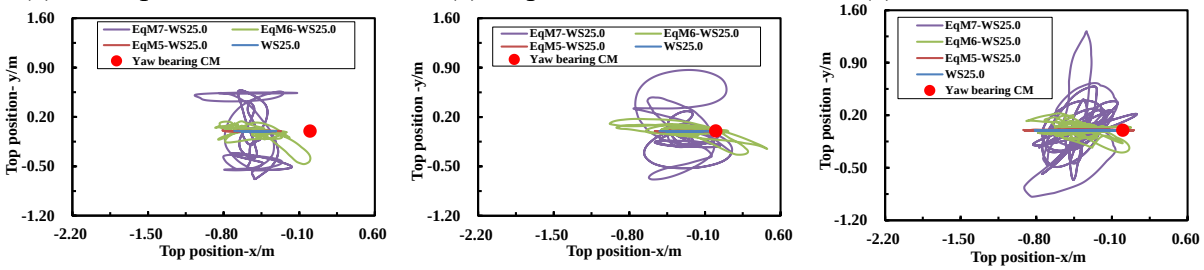

(b) Monopile-WS25.0 m/s (d) Tripod-WS25.0 m/s (f) Jacket-WS25.0 m/s

Figure 15: Time domain response of *x* and *y* positions of the tower top to relative to yaw bearing CM

513 It is observed from Figure 15 that the tower top's change in position in the *x* and
514 *y* directions under the earthquake was more intense.

515 The trajectories of the tower top's change in position are closer to the centroid of
516 yaw bearing. The distance of these trajectories from the center of mass also reflects the
517 stability of the support structure. This phenomenon can be attributed to the pitching
518 system of the wind turbine. When the operational wind speed of the OWT exceeds rated
519 wind speed (11.4 m/s), the OWT wind loads decrease with increase in the wind speed.
520 The obvious reason for the decreases in the position of the tower top to relative to yaw
521 bearing CM under earthquakes are caused by the reduction in wind loads.

522 The amplitude of the tower top's change in position increases with the intensity of
523 the earthquake. Furthermore, the trajectory of the tower top's change in position is a
524 straight line in the fore-aft direction when it is not under any earthquake. The
525 amplification of the tower top's change in position caused by the M 5 earthquake is not
526 obvious but the increase caused by M 6 and M 7 earthquakes is apparent. The trajectory
527 of the change in position diverges and increases in magnitude along the *x* and *y*
528 directions.

The trajectory of change in position of monopile is farther to the centroid of a yaw bearing under seismic loads, and the trajectory of change in position of the tripod is closer. The degree of divergence of the trajectory of the tower top's change in position for a tripod under earthquakes is more significant than monopile and jacket, but the value of the relative position is smaller from the time-domain curve. Under the load predicted in rated wind speed of 11.4 m/s and M 7 earthquake, the peak position of the tripod is 1.42 m, and the monopile is 1.8 m, with a difference of 26.8%. This phenomenon proves that the time-domain response usually adopts a relative position approach, which takes the centroid of the yaw bearing as the origin. The tower top's relative position trajectory of the tripod is closer to the centroid of yaw bearing. Therefore, structural stability analysis from time-domain curve may lead to one-sided results.

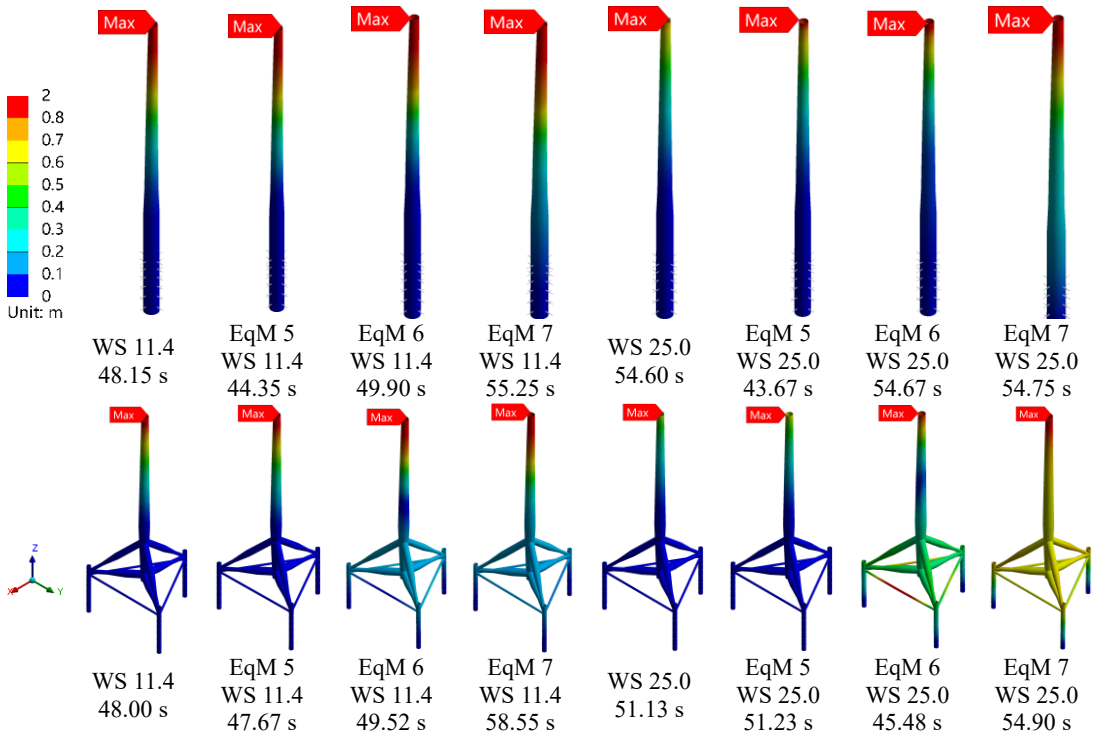

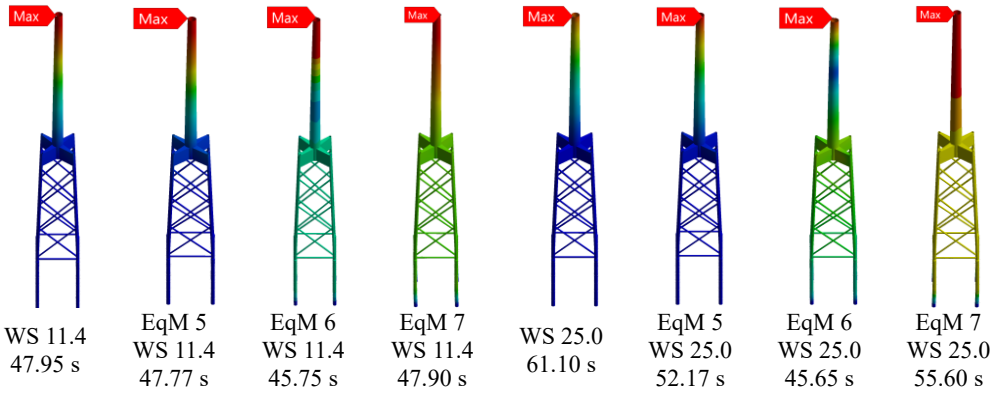

Figure 16: Displacement contours of different support structures for the different load conditions

The displacement contours of the monopile, tripod and jacket OWTs under different environmental and seismic conditions are presented in Figure 16. In the subgraphs, "EqM7+WS25+61.10s" means earthquake magnitude 7 combined with wind speed 25.0 m/s and response time at 61.10 s. For each of these cases, the maximum deformation over the simulation is achieved at the given time instant presented at the bottom of the corresponding sub-figure. With an increase in earthquake magnitude, the displacement gradually increases. Because of the pitching system, the support structure suffers from a more significant wind load under the rated (11.4 m/s) wind condition compared to the cut-out (25 m/s) wind speed condition. Aerodynamic loads can effectively decrease the structural deformation under an earthquake by providing an equivalent damping. This phenomenon is more clearly observed from the displacement contours of the tripod and jacket under the M 7 earthquake event.

The variation range of the monopile OWT's tower top displacement is the largest between the results of these three support structures when an earthquake is considered. The maximum displacement is larger than 0.8 m and increases with earthquake magnitude. The deformation of the tower gradually decreases from top to bottom. A similar phenomenon is observed for the tripod model. The displacement of the mean

558 sea level is smaller than 0.1 m for both cases without an earthquake or with just the M
559 5 earthquake.

560 The displacements of the tripod at MSL are 0.4 m and 0.6 m for M6 and M7
561 earthquakes, respectively,. The response trend of the jacket is consistent with that of the
562 tripod model. However, it is noted that the tower displacement of the jacket OWT is
563 above 0.7 m and significantly larger than that of the tripod. This is because the SSI
564 effects have more significant consequence on the jacket model, which leads to a smaller
565 natural frequency of the OWT's second mode. Under the excitation of the M7
566 earthquake, the tower vibration is more severe as the second mode of the support
567 structure is activated. This phenomenon may be due to the high structural stiffness of
568 the transition piece of the jacket and it corresponds to the subsequent stress research
569 results.

570 *5.1.2 Equivalent stress*

571 The phenomenon of stress concentration probability occurs on the tripod and
572 jacket OWTs. Therefore, the maximum peak and average equivalent stress of each
573 model are calculated, as shown in Table 7. The maximum stress contours are shown in
574 Figure 17.

575 Table 7 Maximum local and total equivalent stress of support structure

Loads condition		WS11.4	WS25.0	EqM5-WS11.4	EqM5-WS25.0	EqM6-WS11.4	EqM6-WS25.0	EqM7-WS11.4	EqM7-WS25.0
Monopile	Maximum (MPa)	91.3	48.6	94.8	53.9	126.1	115.5	193.7	195.8
		-	-	3.9%	10.9%	38.1%	137.5%	112.3%	302.8%
	Average (MPa)	28.9	15.4	29.3	15.9	33.3	21.6	38.0	25.7
		-	-	1.3%	3.2%	15.1%	40.2%	31.5%	66.7%
Tripod	Maximum (MPa)	179.7	96.0	183.6	105.4	253.9	235.7	454.1	441.0
		-	-	2.1%	9.8%	41.3%	145.6%	152.7%	359.4%

	Average (MPa)	9.8	5.2	10.2	6.0	15.4	13.3	22.9	18.9
		-	-	4.5%	14.7%	58.2%	155.4%	135.3%	261.6%
Jacket	Maximum (MPa)	394.9	213.2	401.5	234.2	605.9	535.1	1142.8	1118.2
		-	-	1.7%	9.9%	53.4%	151.0%	189.4%	424.6%
	Average (MPa)	9.7	5.3	10.0	5.8	13.7	11.9	16.6	14.4
		-	-	2.9%	10.9%	40.7%	125.6%	70.3%	172.9%

Table 7 presents the maximum stress and the average stress at the total nodes of each model under the earthquake. The seismic loads cause the increase of the stress amplitude. The trend of structural stress under earthquakes is displayed by the fluctuation of stress amplitude with the change of seismic load.

The equivalent stress under the rated wind speed (11.4 m/s) is larger than cut-out wind speed (25 m/s), which corresponds to the above displacement response. The equivalent stress increases violently with an increase in earthquake magnitude. With the wind load changing from cut-out (25 m/s) to rated (11.4 m/s) wind speeds, the amplitude of stress from OWT suffering from earthquakes is less.

The stress of each support structure under earthquake is compared against. The jacket OWT has the largest maximum local equivalent stress, while the monopile OWT has the smallest. Also, the jacket OWT has the smallest average total equivalent stress, and the monopile OWT has the largest. This phenomenon proves that the external load leads to the overall bending deformation of the monopile OWT. The high stiffness of the tripod and jacket substructures ensures the stability of the structure, but they lead to the increase in local stress. Therefore, the stress contours of each model at peak time are investigated.

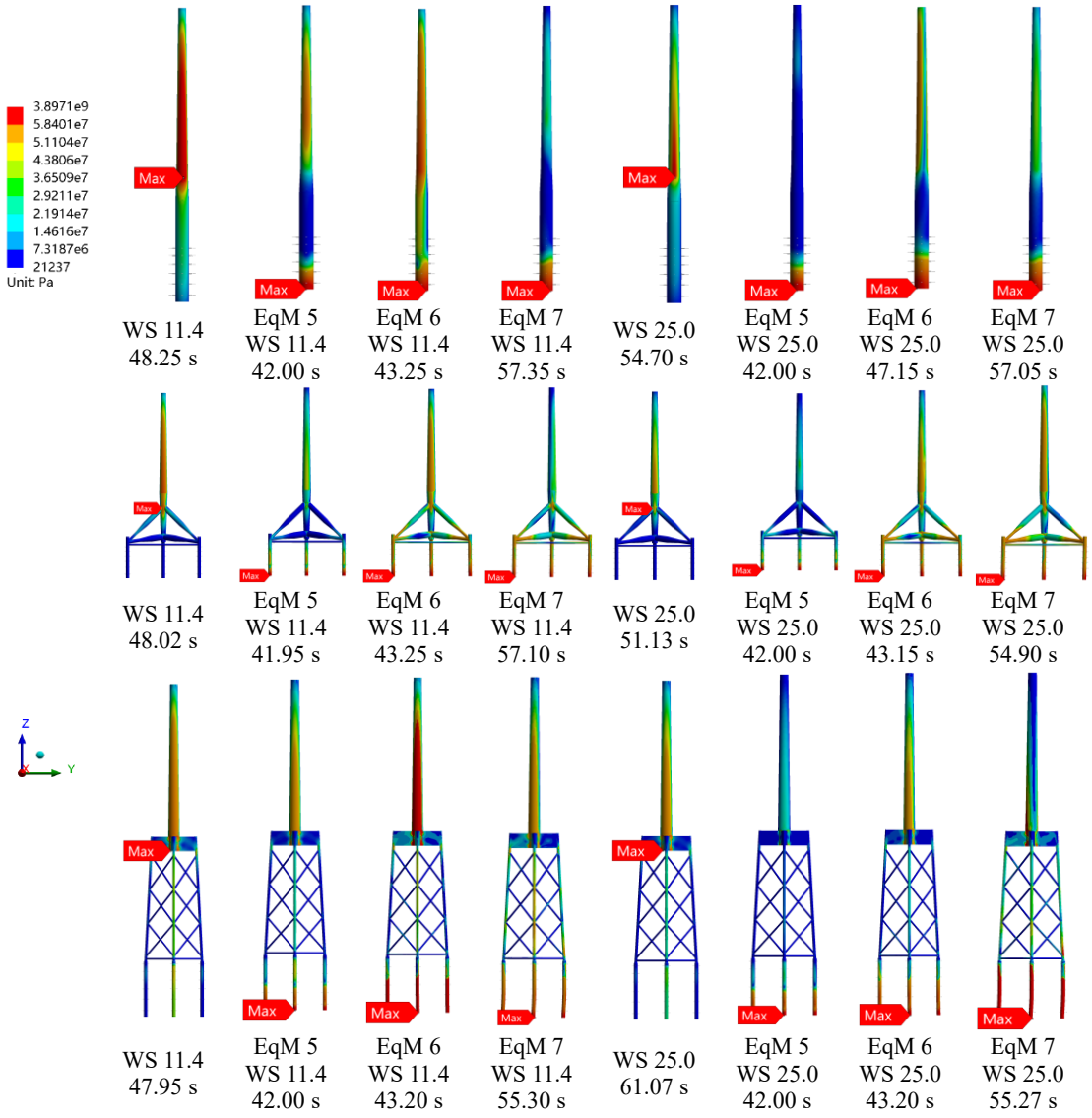

Figure 17: The equivalent stress contours for different earthquake and wind conditions

The stress contours of monopile, tripod and jacket OWTs are presented in Figure 17. The maximum stress recorded throughout the simulation is achieved at the given time instances presented at the bottom of the corresponding sub-figure. The earthquake causes the stress of support structures to enormously increase. The stress of piles significantly increases with earthquake magnitude. The peak time of stress is close to the peak time of the earthquake, but it is delayed by several seconds.

The tower base of the monopile OWT has the largest stress without an earthquake. The most intense stress location on the tripod is the connection between the central pile

and the sub pile. The most intense stress location on the jacket is the connection point between the tower and the transition piece. The pile stress along the *x* direction is slightly larger than others. The X-braces connections of the jacket experience stress increase.

5.1.3 Response of pile foundation

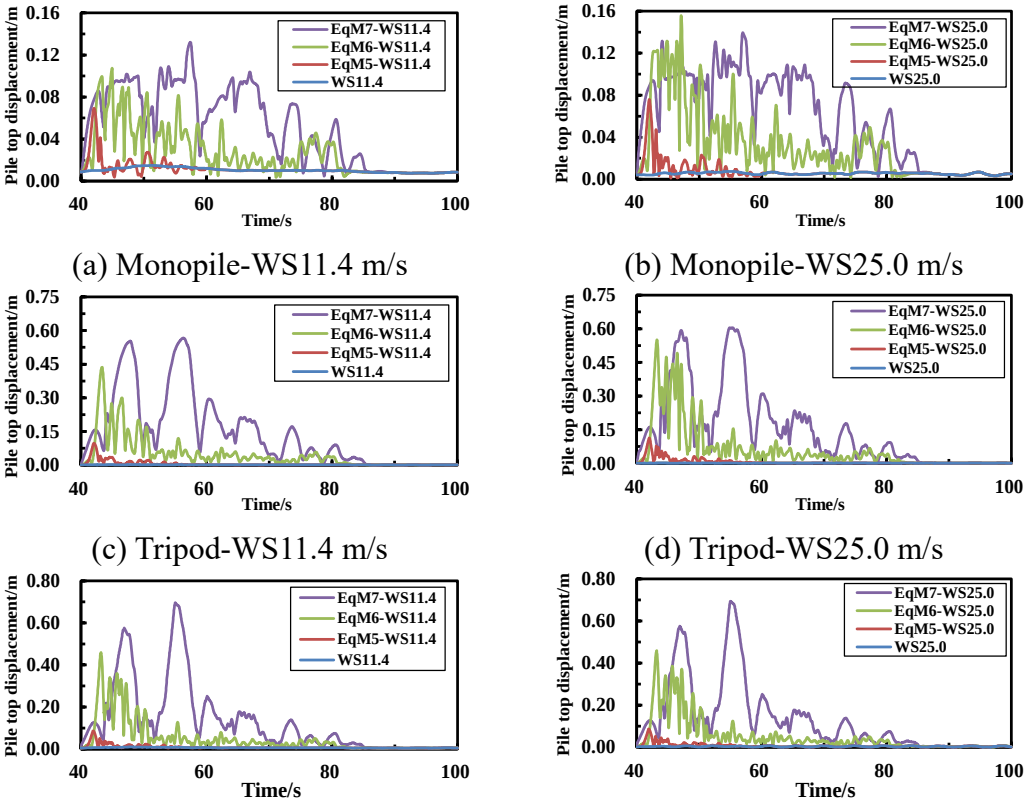

(a) Monopile-WS11.4 m/s (b) Monopile-WS25.0 m/s

(c) Tripod-WS11.4 m/s (d) Tripod-WS25.0 m/s

(e) Jacket-WS11.4 m/s (f) Jacket-WS25.0 m/s

Figure 18: Time domain response of displacement of the pile

As shown in Figure 18, the displacement of piles is increased, the piles suffer from the earthquake, and the duration of the vibration is proportional to the ground motion.

For the monopile OWT, the maximum displacement of the pile is 0.139 m under the cut-out (25.0 m/s) wind speed and M 7 earthquake excitations. The maximum displacement of the pile of the tripod and jacket OWT under the same earthquake excitations is 0.605 m and 0.694 m, respectively. Under the rated (11.4 m/s) wind speed

and M 7 earthquake excitations, the corresponding values of monopile, tripod and jacket OWT are 0.132 m, 0.566 m and 0.696 m, respectively. This phenomenon shows that the displacement of the pile is mainly affected by the seismic loads, rather than the wind load.

The piles generally experience very little displacement in the absence of an earthquake. The displacement of the pile for all the structural support types is close to each other's under different wind loads. This phenomenon proves that the displacement of the pile can be ignored when there is no earthquake. The piles of jacket OWT are smaller in diameter and have thinner wall thickness than monopile and tripod. The pile displacement of the jacket is larger than others under the same earthquake, but the structural responses of the support structure are more stable. Consequently, the pile of OWTs with a small diameter and thin wall thickness may rely on the larger stiffness provided collectively by substructures to improve the stability.

6. Conclusions

In this study, dynamic behaviours of 10 MW OWTs with different support structures have been investigated under various environmental loadings including earthquake excitations. The shell FEMs of monopile, tripod and jacket support structures are developed in ANSYS and the nonlinear SSI effects are examined using the Winkler springs, whose stiffness is defined using *p-y* and *Q-z* curves. The time-varying responses of wind and the hydrodynamic loads induced by wave and current actions on each structure are calculated in FAST and AQWA, respectively. Earthquake events with different magnitudes are examined. The dynamic responses of the support

structures are predicted by using the finite element method. Based on the simulation results and discussions obained in this investigation, the following conclusions are drawn:

(1) The tower top displacement of jacket OWTs under wind loads from rated wind speed (11.4 m/s) and M 6 earthquake excitations is the maximum of tower top displacement caused by seismic loads in the investigation with a value of 1.88 m. The displacement increment of jacket OWTs under the 25.0 m/s wind load and M 7 earthquake excitations is the maximum increment of tower top displacement caused by seismic loads in the investigation with a value of 0.54 m. The maximum tower top displacement of the OWT with different support structure increases with the change in earthquake magnitude, but the trend of amplitude variation is not linear with earthquake magnitude.

(2) The amplitude of relative positions in the *y* direction is almost approaching 0 m without seismic loads. The change in relative position of a monopile OWT is farthest from the centroid of a yaw bearing under seismic loads, while the trajectory of the tripod is the nearest. The divergence in the degree of trajectory for the tower top of the tripod under earthquake is more significant than for both monopile and jacket, but the relative position is smaller. The tripod structure is more stable but more sensitive to seismic load. The tower top's change in relative position or the tripod is closer to the centroid of yaw bearing. Therefore, structural stability analysis from time-domain may lead to one-sided results.

(3) The increments of tower top displacement by M 7 earthquakes are about 36%

656 and 71% under 11.4 m/s and 25.0 m/s wind loads, respectively. When the wind load
657 changes from cut-out (25 m/s) to rated (11.4 m/s) wind speeds, the structural stress
658 amplitude under an earthquake is less, but the amplitude of displacement is more
659 intense. The external load leads to the overall bending deformation of the monopile
660 structure. The maximum tower top displacements of the tripod and jacket OWTs, which
661 are smaller than the monopile, are 1.42 m and 1.95 m under external loads, respectively.
662 The maximum local stresses of the tripod and jacket OWTs, which are much more than
663 the monopile, are 454.1 MPa and 1142.8 MPa under wind loads from rated wind speed
664 (11.4 m/s) and M 7 earthquake excitations, respectively. The transition piece of the
665 tripod and jacket OWTs ensures that the overall stiffness and stability of the structure
666 remains intact, but it leads to an increase in local stress.

667 (4) The stress response of piles is the most intense under earthquakes. The stress
668 response of pile foundation becomes more intense with a severer earthquake magnitude.
669 Taking the case of M 7 earthquake as an example, the peak time of M 7 earthquake
670 excitations is 55.00 s. The peak times of pile displacement for monopile, tripod and
671 jacket OWT are 57.43 s, 56.30 s and 55.90 s under M 7 earthquake excitations,
672 respectively. The peak time of stress is close to when the ground displacement reaches
673 the peak, but the phenomenon is delayed by several seconds. The displacement of pile
674 caused by earthquake is proportional to magnitude. The maximum pile displacement of
675 monopile, tripod and jacket OWT are 0.14 m, 0.60 m and 0.70 m under M 7 earthquake
676 excitations, respectively. The displacement of the pile foundation is mainly caused by
677 seismic load and is less affected by wind. The pile diameter and wall thickness directly

affect the seismic dynamic response on the support structure of the wind turbine.

Acknowledgments

The authors would like to acknowledge the financial supports from the National Natural Science Foundation of China (grant numbers: 51976131, 52106262), Zhejiang Provincial Natural Science Foundation of China (grant number: LQ22E090001) and the Shanghai University Science and Technology Innovation Action Plan Local University Capacity Building Project (grant number: 19060502200).

References

[1] GWEC, Global Wind Report 2021, Global Wind Energy Council, Brussels, 2021.

[2] J. Tempel, N. Diepeveen , D. Salzmann, W. Vries, Design of Support Structures for Offshore Wind Turbines, Transactions on State of the Art in Science and Engineering. 44 (2010) 560-591.

[3] M. Ferguson, Opti-OWECS final report Vol. 4: a typical design solution for an offshore wind energy conversion system, Institute for Wind Energy. Delft University of Technology. 1998.

[4] C. Pérez-Collazo, D. Greaves, G. Iglesias, A review of combined wave and offshore wind energy, Renewable and Sustainable Energy Reviews. 42 (2015) 141-153.

[5] J. Koh, E. Ng, Downwind offshore wind turbines: opportunities, trends and technical challenges, Renewable and Sustainable Energy Reviews. 54 (2016) 797-808.

[6] Z. Wang, C. Jiang, A. Qian, C. Wang, The key technology of offshore wind farm and its new development in China, Renewable and Sustainable Energy Reviews. 13 (2009) 216-222.

[7] S. Bisoi, S. Haldar, Design of monopile supported offshore wind turbine in clay considering dynamic soil-structure-interaction, Soil Dynamics and Earthquake Engineering. 73 (2015) 103-117.

[8] R. Risi, S. Bhattacharya, K. Goda, Seismic performance assessment of monopile-supported offshore wind turbines using unscaled natural earthquake records, Soil Dynamics and Earthquake Engineering. 109 (2018) 154-172.

[9] Det Norske Veritas, Guidelines for design of wind turbines, Copenhagen: Wind

Energy Department of Risø National Laboratory. 2002.

[10] L. Germanischer, Guideline for the certification of wind turbines, Hamburg: Germanischer Lloyd. 2003.

[11] N. Agbayani, A technical overview of ASCE/AWEA RP2011: Recommended practice for compliance of large land-based wind turbine support structures, Structures Congress. (2014) 1759-1770.

[12] L. Arany, S. Bhattacharya, J. Macdonald, S. Hogan, Closed form solution of eigen frequency of monopile supported offshore wind turbines in deeper waters incorporating stiffness of substructure and SSI, Soil Dynamic Earthquake Engineering. 83 (2016) 18-32.

[13] A. Patil, S. Jung, O. Kwon, Structural performance of a parked wind turbine tower subjected to strong ground motions, Engineering Structures. 120 (2016) 92-102.

[14] M. Hussan, M. Rahman, F. Sharmin, D. Kim, J. Do, Multiple Tuned Mass Damper for Multi-Mode Vibration Reduction of Offshore Wind Turbine Under Seismic Excitation, Ocean Engineering. 160 (2018) 449-460.

[15] L. Zhang, X. Li, Dynamic analysis of a 5-MW tripod offshore wind turbine by considering fluid-structure interaction, China Ocean Engineering. 31 (5) (2017) 559-566.

[16] Y. Liu, C. Hu, M. Sueyoshi, S. Yoshida, H. Iwashita, M. Kashiwagi, Motion response characteristics of a Kyushu-University semi-submersible floating wind turbine with trussed slender structures: experiment vs. numerical simulation. Ocean Engineering. 232 (2021) 109078.

[17] V. Anand, S. Kumar, Seismic Soil-structure Interaction: A State-of-the-Art Review, Structures. 16 (2018) 317-326.

[18] M. Asareh, I. Prowell, J. Volz, W. Schonberg, A computational platform for considering the effects of aerodynamic and seismic load combination for utility scale horizontal axis wind turbines, Earthquake Engineering and Engineering Vibration. 15 (1) (2016) 91-102.

[19] M. Asareh, I. Prowell, Seismic loading for FAST (No. NREL/SR-5000-53872), National Renewable Energy Laboratory, Golden, 2011.

[20] Y. Yang, K. Ye, C. Li, C. Michailides, W. Zhang, Dynamic behavior of wind turbines influenced by aerodynamic damping and earthquake intensity, Wind Energy. 21 (1) (2018) 1-17.

[21] S. Jalbi, S. Bhattacharya, Minimum foundation size and spacing for jacket supported offshore wind turbines considering dynamic design criteria, Soil Dynamics and Earthquake Engineering. 123 (2019) 193-204.

[22] A. Ali, R. Risi, A. Sextos, Seismic assessment of wind turbines: How crucial is rotor-nacelle-assembly numerical modeling, Soil Dynamics and Earthquake Engineering. 141 (8) (2021) 106483.

[23] N. Bazeos, G. Hatzigeorgiou, I. Hondros, H. Karamaneas, D. Karalalis, D. Beskos, Static, seismic and stability analyses of a prototype wind turbine steel tower, Engineering Structures. 24 (8) (2002) 1015-1025.

[24] A. Sadowski, A. Camara, C. Málaga-Chuquitaype, K. Dai, Seismic analysis of a tall metal wind turbine support tower with realistic geometric imperfections,

Earthquake Engineering and Structural Dynamics. 46 (2) (2016) 201-219.

[25] Y. Xu, Q. Ren, H. Zhang, W. Shi, Collapse analysis of a wind turbine tower with initial-imperfection subjected to near-field ground motions, Structures. 29 (9) (2021) 373-382.

[26] H. Yang, Y. Zhu, Q. Lu, J. Zhang, Dynamic reliability based design optimization of the tripod sub-structure of offshore wind turbines, Renewable Energy. 78 (2015) 16-25.

[27] J. Lana, P. Junior, C. Magalhes, A. Magalhes, A Junior, M. Ribeiro, Behavior study of prestressed concrete wind-turbine tower in circular cross-section, Engineering Structures. 227 (2021) 111403.

[28] ANSYS Inc, ANSYS 19.5 ANSYS mechanical APDL, Canonsburg, 2019.

[29] T. Ishihara, M. Sarwar, Numerical and Theoretical study of seismic response of wind turbines, in: Proceeding of European Wind Energy Conference ,2008.

[30] R.K. Tesser, L.P. Laercio, F. Dupros, P. Navaux, C. Mendes, Improving the Performance of Seismic Wave Simulations with Dynamic Load Balancing, in: the 2014 22nd Euromicro International Conference on Parallel, Distributed, and Network-Based Processing. IEEE Computer Society, 2014.

[31] H. Ma, D. Zhang, Seismic response of a prestressed concrete wind turbine tower, International Journal of Civil Engineering. 14 (8) (2016) 561-571.

[32] D. Witcher, Seismic analysis of wind turbines in the time domain, Wind Energy. 8 (1) (2010) 81-91.

[33] W. Nie, Q. Liu, Dynamic Analysis of Offshore Structures, Harbin Engineering

University Press, Harbin, China, 2002.

[34] M. AlHamaydeh, S. Barakat, O. Nassif. Optimization of quatropod jacket support structures for offshore wind turbines subject to seismic loads using genetic algorithms, in: the 5th International Conference on Computational Methods in Structural Dynamics and Earthquake Engineering. Crete Island, Greece, 2015 3505–3513.

[35] M. Achmus, Y. Kuo, K. Abdel-Rahman, Behavior of monopole foundation under cyclic lateral load, Comput Geotech. 36 (5) (2009) 725-35.

[36] L. Andersen, M. Vahdatirad, M. Sichani, J. Sorensen. Natural frequencies of wind turbines on monopole foundations in clayey soils-a probabilistic approach, Comput Geotech. 2012 (43) (2012) 1-11.

[37] L. Germanischer. Guideline for the certification of offshore wind turbines. Hamburg, Germany, 2005.

[38] C. Sun, V. Jahangiri, Bi-directional vibration control of offshore wind turbines using a 3D pendulum tuned mass damper - ScienceDirect, Mechanical Systems and Signal Processing. 105 (2018) 338-360.

[39] H. Ma, J. Yang, L. Chen, Effect of scour on the structural response of an offshore wind turbine supported on tripod foundation, Applied Ocean Research. 73 (2018) 179-189.

[40] C. Bak, R. Bitsche, A. Yde, T. Kim, Light Rotor: The 10MW Reference Wind Turbine, in: the European Wind Energy Association European Wind Energy Conference and Exhibition. Copenhagen, European Wind Energy Association,

(2012) 16-19.

[41] C. Bak, F. Zahle, R. Bitsche, T. Kim, A. Yde, L. Henriksen, M. Hansen, M. Gaunaa，A. Natarajan, The DTU 10MW Reference Wind Turbine. Fredericia, Danish Wind Power Research, 2013.

[42] K. Oh, J. Kim, J. Lee, Preliminary evaluation of monopile foundation dimensions for an offshore wind turbine by analyzing hydrodynamic load in the frequency domain, Renewable Energy. 54 (2013) 211-218.

[43] W. Shi, J. Han, C. Kim, D. Lee, H. Shin, H. Park, Feasibility study of offshore wind turbine substructures for southwest offshore wind farm project in Korea, Renewable Energy. 74 (2015) 406-413.

[44] J. Velarde, E. Bachynski, Design and fatigue analysis of monopile foundations to support the DTU 10 MW offshore wind turbine, Energy Procedia. 137 (2017) 3-13.

[45] E. Estrada, O. Danguillecourt, J. Ocampo, A. Lopez, P. Camacho, B. Sariñana, J. Portela, Considerations for the structural analysis and design of wind turbine towers: A review, Renewable and Sustainable Energy Reviews. 137 (2021) 110447.

[46] U.S. Department of the Interior, Technology white paper on wind energy potential on the U. S. outer continental shelf, America, 2006.

[47] Y Yang, C Li, M Bashir, Analysis of the dynamic behaviour of 10 MW bottom fixed offshore wind turbines. in: 3rd International Conference on Offshore Renewable Energy, Glasgow, 2018.

[48] E. Minguez, A. Kolios, F. Brennan, Multi-criteria assessment of offshore wind turbine support structures, Renewable Energy. 36 (2011) 2831-2837.

[49] J. Häfele, C. Gebhardt, R. Rolfes, Innovative design of a hybrid-type jacket for 10MW turbines, INNWIND. EU, Deliverable D 4 (2017).

[50] M.J. Kaiser, B. Snyder, Offshore wind energy installation and decommissioning cost estimation in the US outer continental shelf. Louisiana, Energy Research Group LLC, (2010).

[51] K. Thomsen, Offshore wind: a comprehensive guide to successful offshore wind farm installation. Academic Press, (2014).

[52] L. Seung, J. González, J. Lee, Y. Kim, K. Park, S. Han, Structural topology optimization of the transition piece for an offshore wind turbine with jacket foundation, Renewable Energy. 85 (2016) 1214-1225.

[53] American Petroleum Institute, Recommended Practice for Planning, Designing and Constructing Fixed Offshore Platforms-Working Stress Design. API Publishing Services, Washington D.C, 2003.